ACS OMEGA

http://pubs.acs.org/journal/acsodf

Article

Triptycene-Based and Schiff-Base-Linked Porous Networks: Efficient Gas Uptake, High CO_2/N_2 Selectivity, and Excellent Antiproliferative Activity

Akhtar Alam, Snehasis Mishra, Atikur Hassan, Ranajit Bera, Sriparna Dutta, Krishna Das Saha, and Neeladri Das*

Cite This: *ACS Omega* 2020, 5, 4250−4260

Read Online

ACCESS | Metrics & More | Article Recommendations | Supporting Information

ABSTRACT: A set of unique triptycene-based and organic Schiff-base-linked polymers (**TBOSBL**s) are conveniently synthesized in which triptycene motifs are connected with 1,3,5-triformylphloroglucinol units via Schiff-base linkages. **TBOSBL**s are amorphous, thermally stable with a reasonable surface area (SA_{BET} up to 649 m^2/g), and have abundant nanopores (pore size < 100 nm). **TBOSBL**s are good sorbents for small gas molecules (such as CO_2, H_2, and N_2) and they can selectively capture CO_2 over N_2. Additionally, **TBOSBL**s show superior antiproliferative activity against human colorectal cancer cells relative to previously reported covalent organic frameworks (COFs). The mechanism of cell death is also studied elaborately.

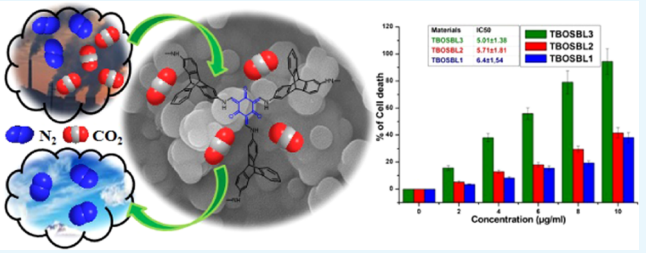

1. INTRODUCTION

The term "cancer" is usually associated with a disease wherein there is an abnormal cell growth in a certain body organ.[1] Cancer is a potentially life-threatening disease that is usually associated with a specific body part but may subsequently spread to other parts of the body. According to the World Health Organization (WHO), "Cancer is the second leading cause of death globally, and was responsible for an estimated 9.6 million deaths in 2018".[2] Based on its origin, cancer can be classified by oncologists as carcinomas, sarcomas, leukemia, and lymphomas.[3] Uncontrolled growth of cancer cells is seen most commonly in lungs, followed by breast, colon/rectum, prostate, skin, and stomach.[2] As far as cancer mortality is concerned, colorectal cancer ranks second after lung cancer. With the current advancement in medical sciences, prevention of death due to cancer is possible, if the disease is diagnosed and treated at an early stage. Among others, chemotherapy is a common mode of treatment. In general, cancer treatment is expensive requiring costly medications. Moreover, carcinoma cells may become resistant to prevalent chemotherapy by a mechanism called "multi-drug resistance" (MDR). Therefore, contemporary research demands design, development, and screening of new compounds/molecules/materials with antiproliferative activity against various cancer cells.[4,5]

In present-day research, there is also a lot of research interest in exploring biomedical applications of porous materials.[5] Such applications include, but are not limited to, chemotherapy, drug delivery, bioimaging, tissue engineering, and others.[6−9] In the context of porous materials, porous organic polymers (POPs) are highly cross-linked macromolecular frameworks containing lighter elements such as hydrogen, carbon, nitrogen, and others. Thus, POPs are distinctly different from metal−organic frameworks (MOFs—another class of porous materials) that are inorganic and contain relatively heavier (metal) atoms. In the literature, there are several examples wherein metal-based porous materials, such as zeolites and MOFs, have been considered for biomedical applications.[10] However, the metal-induced toxicity and chemical instability of MOFs make them undesirable candidates for such applications.[11,12] On the other hand, the absence of inherent toxicity of metal atoms and higher chemical stability observed in POPs render them more suitable as candidates for biological studies. Additionally, POPs have high surface areas and tunable porosity, and are usually obtained easily from inexpensive and commercially available monomers. Therefore, the current research trend is to explore the interaction of POPs with biological species.[6] In this field, the exploration of anticancer activities of POPs decorated with various organic functional groups is still in the stage of infancy. Another major application of porous materials is in the domain of carbon dioxide capture and sequestration (CCS).[13,14]

Triptycene is a rigid and structurally robust molecule. Its incorporation as a structural motif in polymeric frameworks has yielded POPs having excellent gas storage ability.[15−18] The paddle wheel orientation of the arene rings in triptycene causes

Received: December 6, 2019
Accepted: February 10, 2020
Published: February 21, 2020

https://dx.doi.org/10.1021/acsomega.9b04160
ACS Omega 2020, 5, 4250−4260

Scheme 1. Syntheses of TBOSBL 1−3

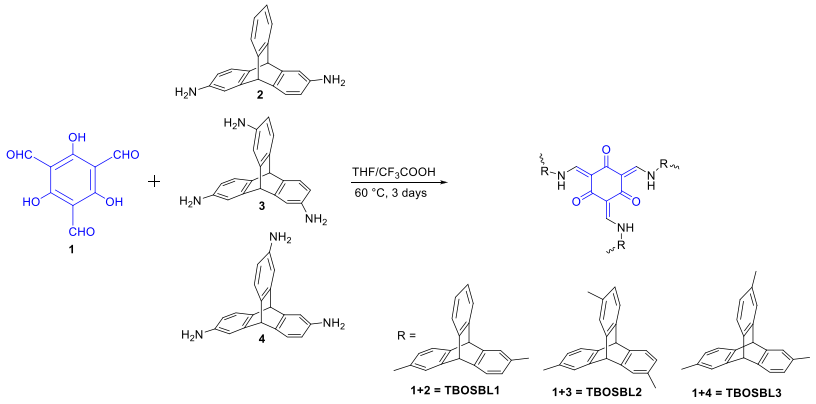

Scheme 2. Structures of TBOSBLs

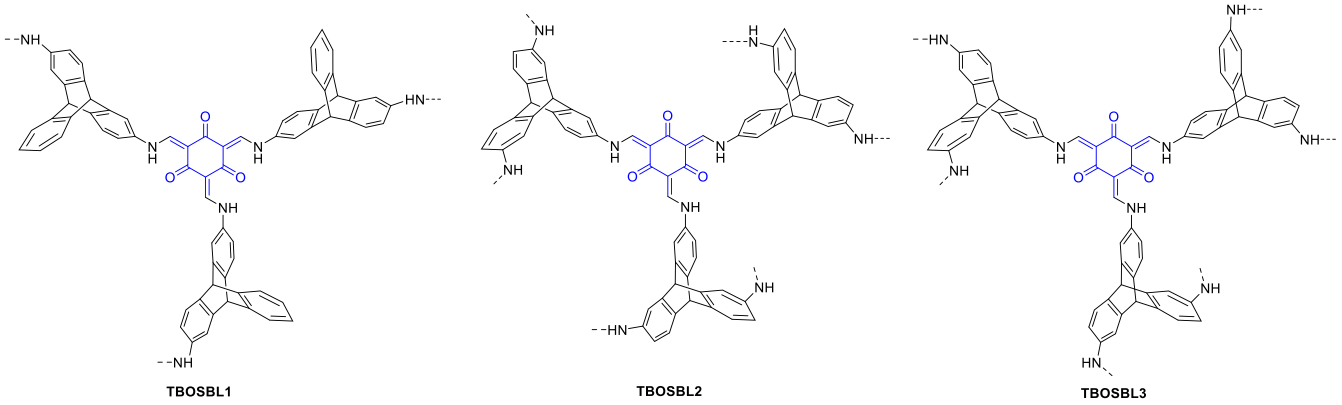

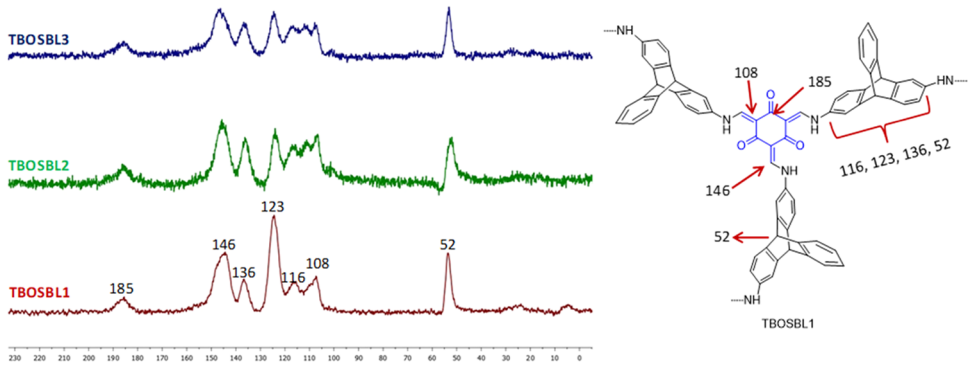

Figure 1. Solid-state ^{13}C CP-MAS NMR spectra of **TBOSBL 1−3**.

these units to pack inefficiently in the polymeric network. This also generates an "internal molecular free volume" (IFV) in the resultant material. The void in the form of IFV, in turn, gives rise to desirable characteristics, such as excellent gas storage capability and high surface areas.[19]

Herein, we report the synthesis of three "triptycene-based and organic Schiff-base-linked" polymers (**TBOSBL**s) prepared via a facile condensation reaction between di- or triaminotriptycene and 1,3,5-triformylphloroglucinol (TFP). The obtained polymeric networks were characterized using Fourier transform infrared (FTIR) and NMR spectroscopy, thermogravimetric analysis (TGA), and X-ray diffraction (XRD). It was anticipated that **TBOSBL**s would be porous since they bear triptycene motifs in the polymeric framework.[20,21] Thus, we have explored their porous properties (surface area/pore size distribution (PSD)) and measured their ability to capture small gas molecules, such as CO_2, H_2, and N_2.

A thorough literature search revealed that polymeric materials derived from polyphenolic units such as phloroglucinol may have considerable potential in research related to cancer therapy.[22,23] This motivated us to explore the anticancer activity of the three **TBOSBL**s reported herein. Further, we have explored whether **TBOSBL**s are apoptotic inducers while proposing a mechanism of cell death. **TBOSBL**s are the only example of triptycene-based POPs whose cytotoxic potential against cancer cells has been studied. The mechanism of cell death was also studied.

https://dx.doi.org/10.1021/acsomega.9b04160
ACS Omega 2020, 5, 4250−4260

2. RESULTS AND DISCUSSION

2.1. Synthesis and Characterization of TBOSBL 1−3.

2,6-Diaminotriptycene (DAT) and 2,6,14- and 2,7,14-triaminotriptycene were synthesized from triptycene based on a protocol reported previously by Chen and co-workers.[24] 1,3,5-Triformylphloroglucinol (TFP) was also synthesized, as described in a literature report.[25] **TBOSBL**s were synthesized via a facile condensation reaction between di- or triamino-triptycene and 1,3,5-triformylphloroglucinol (TFP) in a solution mixture of anhydrous tetrahydrofuran (THF) and trifluoroacetic acid (TFA, 2 mol % in THF) at 60 °C for 3 days (Scheme 1). The resulting precipitate was collected by suction filtration and washed subsequently with tetrahydrofuran, dimethylformamide (DMF), dimethyl sulfoxide (DMSO), water, methanol, acetone, and dichloromethane, separately. The precipitate obtained was washed with various solvents to ensure removal of any unreacted monomers and undesired byproducts, such as soluble small oligomers. The collected powder was then dried at 120 °C under vacuum for 24 h to yield a yellow powder with high yield and insoluble in common organic solvents.

Solid-state ^{13}C cross-polarization magic angle spinning (CP-MAS) NMR spectra were recorded to investigate the formation of **TBOSBL**s, as proposed in Scheme 2. The ^{13}C CP-MAS spectra of **TBOSBL**s are depicted in Figure 1. Taking **TBOSBL1** as a representative example, peaks with different chemical shifts appearing in its NMR spectrum are assigned appropriately in Figure 1. In all three spectra, the strong signal appearing at 52 ppm is assigned to the bridgehead carbons present in the triptycene unit, thereby indicating the incorporation of triptycene motifs in the reaction product. The peaks in the range 116−136 ppm are due to the carbons that constitute the three arene rings present in the triptycene moiety. The band centered at 185 ppm is assigned to deshielded carbonyl carbon atoms, the low-intensity signal at 146 ppm is assigned to the enamine carbon nuclei, and the peak at 108 ppm is due to sp^2 hybridized carbon nuclei of the phloroglucinol unit in the final product. Also, the absence of a unique signal at 191 ppm (due to carbon present in the aldehyde group −CHO of TFP) confirmed that all three aldehyde groups present in triformylphloroglucinol (TFP) molecules reacted completely with aminotriptycenes in the Schiff-base condensation reaction shown in Scheme 1.

FTIR spectra of **TBOSBL**s are shown in Figure 2. The FTIR spectrum of **TBOSBL1** has been described as a representative example. For comparison, the FTIR spectra of the corresponding triptycene-based amine monomer (DAT) and TFP are also depicted in Figure 2. Upon comparing the FTIR spectra of monomers DAT and TFP, and their polymerized product (**TBOSBL1**), it can be concluded that both monomers have reacted completely. In the spectrum of **TBOSBL1**, the absence of the carbonyl (C═O) stretching band characteristic of TFP (1652 cm^{-1}) indicates its consumption in the polymerization reaction and its incorporation in **TBOSBL1**. Formation of enamine linkages in the products is confirmed from the appearance of a high-intensity band at 1290 cm^{-1} due to C−N stretching vibrations. The high-intensity signal at 1448 cm^{-1} is assigned to C−H bending vibrations. The existence of TFP in its keto form (as depicted in Scheme 1) is evident from the appearance of a high-intensity and sharp band at 1586 cm^{-1} in **TBOSBL1** since this is characteristic of C═C bond stretching vibrations observed in the keto form of TFP.[26,27] This is also

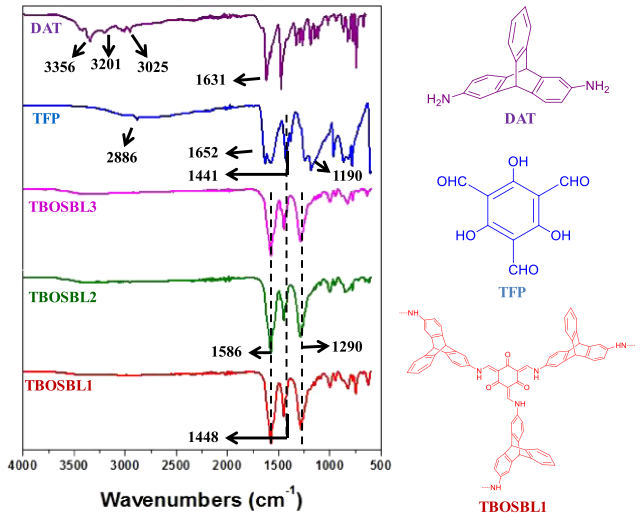

Figure 2. FTIR spectra of 2,6-diaminotriptycene (DAT), TFP, and **TBOSBL**s.

supported by the fact that stretching bands of hydroxyl (in enol form of TFP) are absent in the FTIR spectrum of **TBOSBL1**.

To investigate the structural morphology of **TBOSBL**s, field emission scanning electron microscopy (FE-SEM) was employed. FE-SEM images of **TBOSBL**s at two different magnifications (10.00k× and 50.00k×) are shown in Figure 3. Higher resolution images indicate the presence of uniform spherical particles that have self-assembled to form large aggregated particles. From inspection, in the case of **TBOSBL1**, the spherical particles are dimensionally bigger than those of **TBOSBL2 and TBOSBL3**. As depicted in Scheme 2, **TBOSBL1** is obtained from diaminotriptycene, while the other two **TBOSBL**s are obtained from triamino-triptycenes. Therefore, in the former case (**TBOSBL1**), the extent of polymerization is expected to be lower and the chance of aggregation via H-bonding is more. This might have led to the formation of bigger aggregates in the case of **TBOSBL1**. The grain size of the polymers was estimated from the FE-SEM images, and the average diameter of grains is 400 ± 20, 200 ± 20, and 200 ± 20 nm for **TBOSBL1**, **TBOSBL2**, and **TBOSBL3**, respectively.

The wide-angle X-ray diffraction (WAXD) plots of **TBOSBL**s are shown in Figure 4A. Here, the appearance of a hump (2θ value = 18°) suggests that these polymeric materials are amorphous in nature. The Schiff-base condensation reaction is fast and irreversible, and this leads to the incorporation of bulky and robust three-dimensional (3D) rigid triptycene units. The rigidity of triptycene units prevents efficient packing that leads to materials with loss of crystallinity, as observed in **TBOSBL**s and other previously reported triptycene-based POPs.[20,28] Samples of **TBOSBL 1−3** are subjected to TGA analysis to record the thermal stability of these polymeric materials. TGA experiments were performed under a constant flow of nitrogen gas in the temperature region of 40−800 °C by heating samples at a rate of 10 °C/min. The TGA plot of each **TBOSBL** is shown in Figure 4B. The observed initial weight loss in the temperature range of 325−500 °C is attributed to the thermal degradation of organic functional groups. Overall, **TBOSBL**s may be considered as materials with moderate thermal stability, as observed from the reasonably high thermal degradation temperature (T_d = 10% weight loss under a N_2 atmosphere)

https://dx.doi.org/10.1021/acsomega.9b04160
ACS Omega 2020, 5, 4250−4260

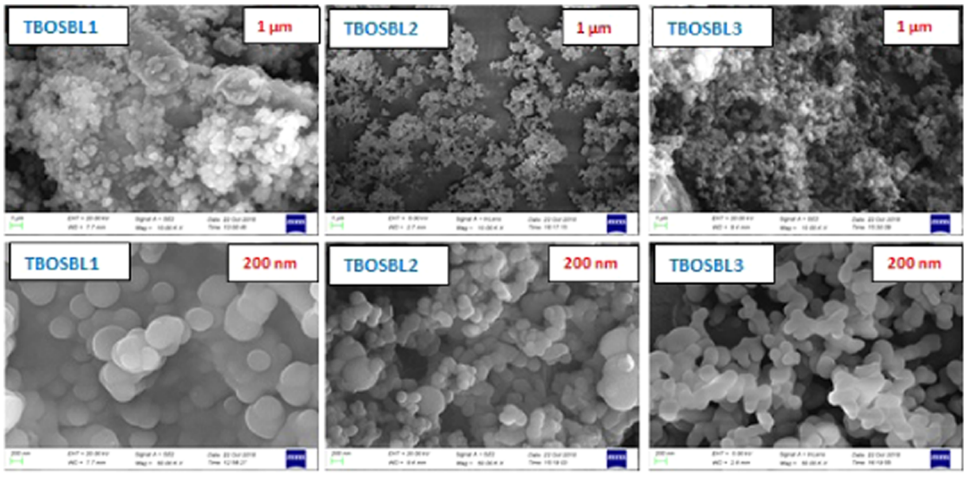

Figure 3. FE-SEM images of **TBOSBL**s.

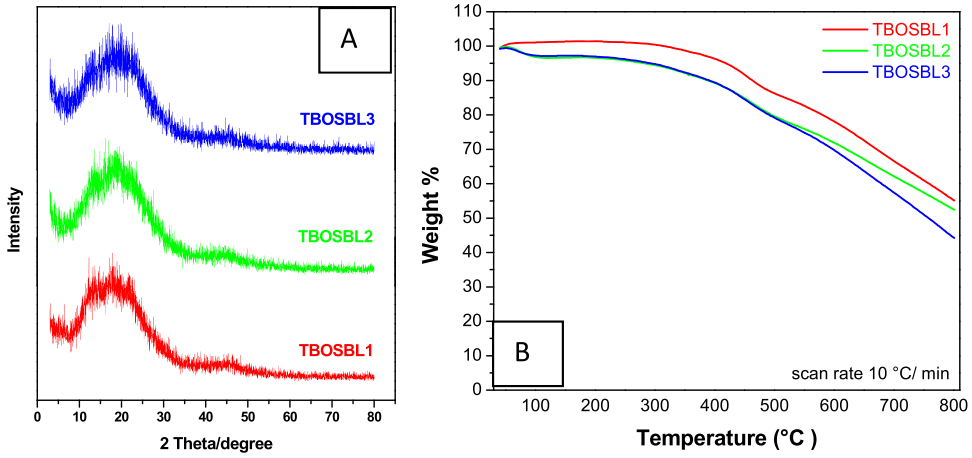

Figure 4. Wide-angle X-ray diffraction (A) and TGA (B) plots of **TBOSBL**s.

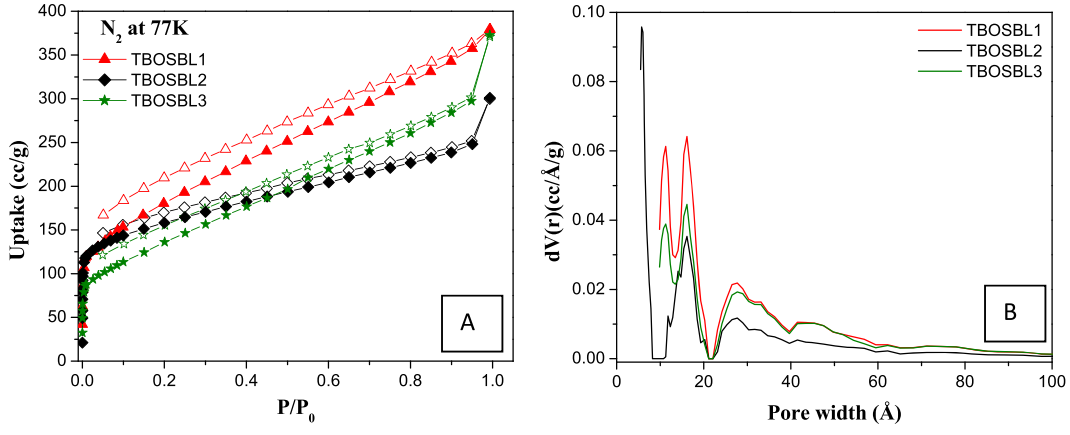

Figure 5. N_2 adsorption−desorption isotherms at 77 K (A) and pore size distribution (B) of **TBOSBL**s.

that varies in the range 388−462 °C. We attribute this desirable feature to the inclusion of robust 3D triptycene units in the polymer framework.[29,30]

2.2. Porosity Measurements. In recent literature related to POPs derived from triptycene-based monomers, it has been observed that such materials have reasonable surface areas with inherent hierarchical porosity for applications such as CO_2 capture and hydrogen storage.[17,31,32] This prompted us to investigate the Brunauer−Emmett−Teller (BET) surface areas and the pore size distributions of **TBOSBL**s. Thus, to determine the porous properties of **TBOSBL**s in detail, N_2 adsorption−desorption isotherms were recorded. The features of N_2 sorption isotherms (collected at 77 K, Figure 5A) of **TBOSBL**s suggest that they may be classified as type-II isotherms.[33] This class of isotherms are usually given by porous materials that have a hierarchical pore structure (coexistence of narrower micropores and relatively wider mesopores). The presence of micropores was evident from the significantly high

https://dx.doi.org/10.1021/acsomega.9b04160
ACS Omega 2020, 5, 4250−4260

Table 1. Pore Properties of TBOSBLs

		[a]	[b]	H_2 at 1 bar (mg/g)	CO_2 at 1 bar (mg/g)			selectivity CO_2/N_2
polymers	SA_{BET} (m^2/g)	SA_{Lang} (m^2/g)[a]	V_{total} (cm^3/g)[b]	77 K	273 K	298 K	Q_{st} (kJ/mol)	273 (298) K
TBOSBL1	649	1051	0.527	19.5	175.6	94.4	35.1	68 (69)
TBOSBL2	570	810	0.384	15.2	149.7	114.4	32.1	106 (63)
TBOSBL3	493	817	0.467	12.9	124.7	96.8	32.7	108 (66)

[a]Surface area of **TBOSBL**s calculated based on the Langmuir model from the N_2 adsorption isotherms (P/P_0 = 0.05−0.35). [b]The total pore volume of **TBOSBL**s calculated at P/P_0 = 0.99.

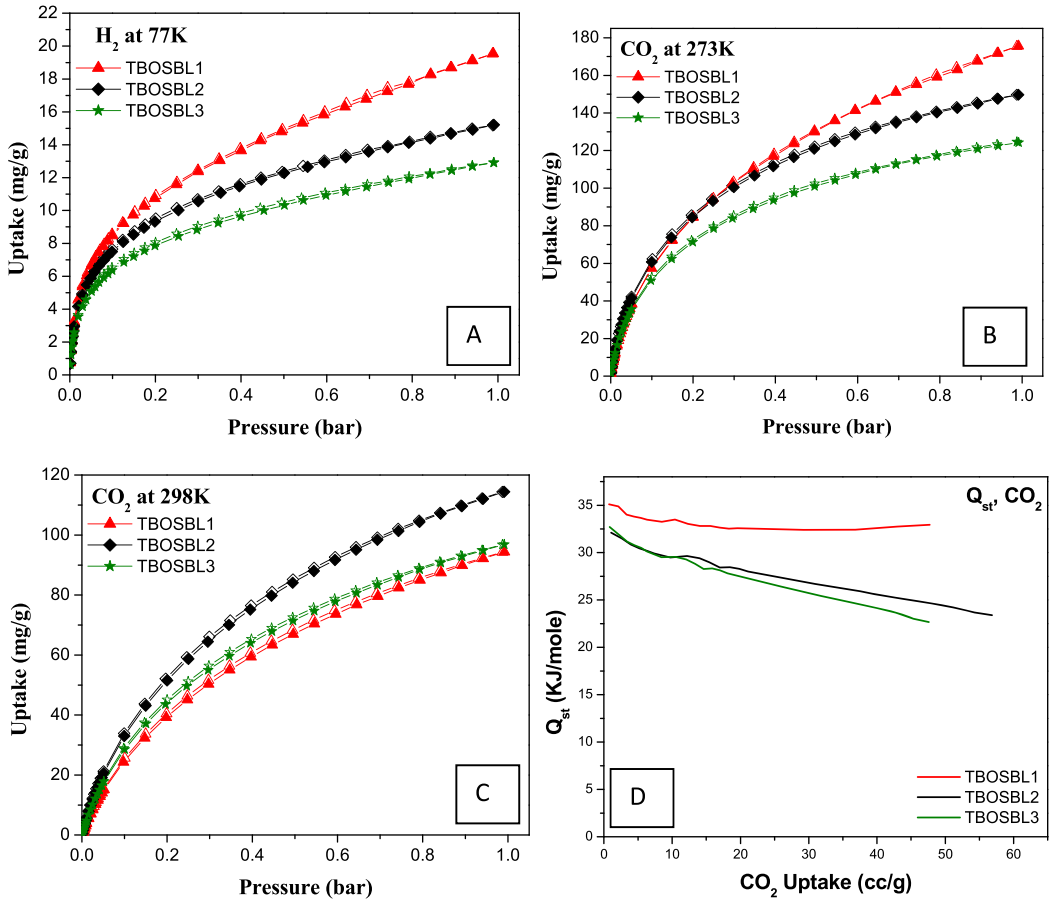

Figure 6. H_2 uptake isotherms at 77 K (A), CO_2 uptake isotherms at 273 K (B) and 298 K (C), and Q_{st} for CO_2 (D) of **TBOSBL**s.

gas uptake in the very low relative pressure range (P/P_0 = 0−0.01), which is depicted as a sharp increase in the corresponding adsorption isotherm.[20] The microporosity present in **TBOSBL**s may be due to the incorporation of the 3D rigid triptycene units in the polymeric linkages.[34] On the other hand, the constant increase in N_2 uptake in the relatively higher partial pressure range (P/P_0 = 0.1−0.99) suggested the existence of mesopores in the polymeric matrix.[35] Using the Brunauer−Emmett−Teller (BET) model, the surface areas were found to be 649 m^2/g (**TBOSBL1**), 570 m^2/g (**TBOSBL2**), and 493 m^2/g (**TBOSBL3**) (Table 1 and Figure S1). The corresponding Langmuir surface areas for **TBOSBL1**, **TBOSBL2**, and **TBOSBL3** are 1051, 810, and 817 m^2/g, respectively (Table 1 and Figure S2). These values are comparable with or better than the surface areas recorded for previously reported microporous materials with Schiff-base linkages. For example, nitrogen-rich microporous and crystalline covalent organic frameworks (COFs) bearing multiple phenolic −OH groups, synthesized via the Schiff-base condensation reaction, have relatively lower SA_{BET} (535 m^2/g for TpPa-1 and 339 m^2/g for TpPa-2) than **TBOSBL1**.[36] Other examples of porous materials with a lower surface area include, but are not limited to, β-ketoenamine-linked COFs (365 m^2/g for DAB-TFP COF),[37] β-ketoenamine-based COFs (567 m^2/g for TAPB-TFP),[38] ionic covalent organic nanosheets ($TpTG_{Cl}$, $TpTG_{Br}$, and $TpTG_I$: 267, 305, and 298 m^2/g, respectively),[39] porous polymer TPDA-1 (545 m^2/g),[40] nitrogen-rich porous organic polymers (104−518 m^2/g for N-POPs),[41] COF materials bearing phloroglucinol building units (223 m^2/g for EDTFP-1),[22] N-rich porous organic polymer methylenedianiline-triformylphloroglucinol (283 m^2/g for MDTFP-1)[23] and triazine-functionalized porous covalent organic frameworks (277 m^2/g for TpTt COF).[25]

As usual, corresponding pore size distribution plots were obtained using the N_2 sorption isotherms and the density functional theory (DFT) method. As predicted from the N_2 isotherms, the pore size distribution (PSD) profile of **TBOSBL**s (Figure 5B) having maxima below and above 2

https://dx.doi.org/10.1021/acsomega.9b04160
ACS Omega 2020, 5, 4250−4260

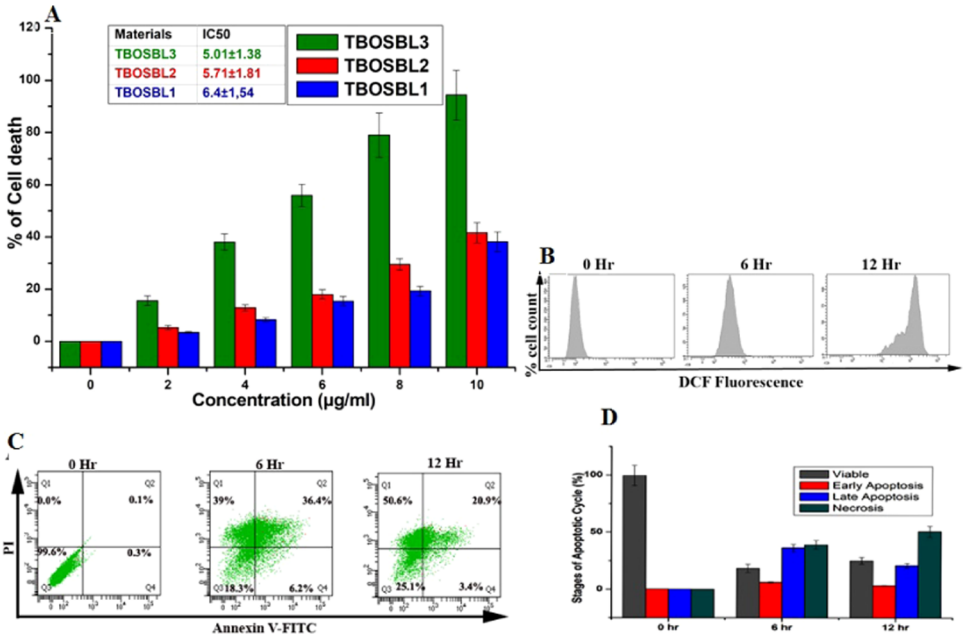

Figure 7. (A) MTT assay data of **TBOSBL**s for 6 h. (B) Reactive oxygen species (ROS) level with time of **TBOSBL3**-treated HCT-116 cells. (C) Graphical presentation of annexin V, FITC/propidium iodide (PI) positive cells with time of treatment with 5 μg/mL **TBOSBL3** by flow cytometry. (D) % of apoptotic HCT-116 cells in a time-dependent manner.

nm confirms that pores are microporous (<2 nm) as well as mesoporous (2−6 nm). The total pore volume of each **TBOSBL** is calculated from the volume of N_2 adsorbed at P/P_0 = 0.99, and this parameter is measured to be 0.527 cm^3/g for **TBOSBL1**, 0.384 cm^3/g for **TBOSBL2**, and 0.467 cm^3/g for **TBOSBL3** (Table 1). These data indicate that both surface area and total pore volume are relatively lower for the POPs (**TBOSBL2** and **TBOSBL3**) derived from the trifunctional triptycenes in comparison with the one (**TBOSBL1**) derived from the bifunctional triptycene monomer. Thus, the porosity and surface area of **TBOSBL**s may be tailored easily by changing the number of reactive sites in the monomers.

2.3. Gas Storage and Selective CO_2 Capture over N_2. Considering the nanoporous nature of **TBOSBL**s, we were interested in studying their ability to act as an adsorbent for small gaseous molecules, such H_2 and CO_2. Therefore, adsorption isotherms of H_2 (at 77 K), CO_2 (at 273, 298 K), and N_2 (at 273, 298 K) were collected at pressures up to 1 bar. The interest in exploring the ability of porous materials to store H_2 gas has assumed importance since hydrogen gas is projected to replace fossil fuel for the global energy requirements, especially in the transportation sector. The H_2 uptake by **TBOSBL**s was found to be in the range of 12.9−19.5 mg/g (Table 1 and Figure 6A). The highest value was observed for **TBOSBL1** (19.5 mg/g or 1.95 wt % at 77 K), and this value was better than those of various microporous organic polymers and COFs—representative examples are triptycene-derived azo polymers (TAP3, 1.44 wt %),[20] azo-Trip (1.46 wt %),[42] 3D ultramicroporous triptycene-based polyimide frameworks (1.41 wt %),[43] carbazole-based porous organic polymers (CPOPs 1.19−1.29 wt %),[44] solvothermally synthesized TpBD (0.7 wt %),[45] TpPa-1, TpPa-2 (1.1, 0.89 wt %),[45] TAPB-TFP (1.08 wt %),[38] and porous porphyrin organic polymers (TpTph, 1.25 wt %).[46] From the above comparison, it is clear that **TBOSBL**s reported herein have improved H_2 uptake capabilities than several microporous polymers and imine-based COFs.

The continuous increase in the concentration of atmospheric CO_2 is a very serious environmental issue. The main challenges are to propose efficient means to remove atmospheric CO_2 and develop technologies for effective carbon dioxide capture and sequestration (CCS). In this context, physisorption of carbon dioxide by porous materials is a widely researched CCS process that has been highlighted in several reviews. It must be mentioned that recent research achievements in this field using porous organic polymers (POPs) for CO_2 capture are noteworthy. An important feature that a porous material must have to qualify for its application in CCS technology is its ability to selectively capture CO_2 in the presence of N_2. Thus, we were also curious to explore the ability of **TBOSBL**s to selectively capture CO_2 over N_2. CO_2 sorption isotherms of **TBOSBL**s were measured at two temperatures 273 K (Figure 6B) and 298 K (Figure 6C) at pressures up to 1 atm. The gravimetric uptake of CO_2 was the highest for **TBOSBL1** (175 mg/g), while it was the lowest for **TBOSBL3** (125 mg/g), as shown in Table 1. Quantitatively, the amount of CO_2 captured by **TBOSBL1** (175 mg/g at 273 K and 1 bar) is better than those by all previously reported imine-based COFs synthesized via the Schiff-base condensation reaction, such as TpPa-1 (153 mg/g),[36] TpBD (84 mg/g),[45] TpPa-F4 (69 mg/g),[47] a freshly activated sample of UCBZ-1 (77 mg/g),[48] and TpTph (163 mg/g).[46] Moreover, this is also higher than the amounts captured by various porous organic polymers, N-rich porous polymers, and triptycene-based microporous polymers, such as N-rich POPs (109 mg/g),[41] amine-based cross-linked porous polymers (66.8 mg/g),[49] nanoporous organic polymers (NOPs, 86−142 mg/g),[50] azo-functionalized microporous organic polymers (77.7−134.8 mg/g),[51] porous covalent triazine polymers (CTPs, 6.6−29.5 mg/g),[52] hexaphenylbenzene-based conjugated microporous polymers (HCMPs, 43−75 mg/g),[53] 3D ultramicroporous triptycene-based polyimide frameworks (149.6 mg/g),[43] and triptycene-derived azo polymers bearing phloroglucinol units (TAPs, 95−150 mg/g).[20] The selectivity of CO_2/N_2 was

https://dx.doi.org/10.1021/acsomega.9b04160
ACS Omega 2020, 5, 4250−4260

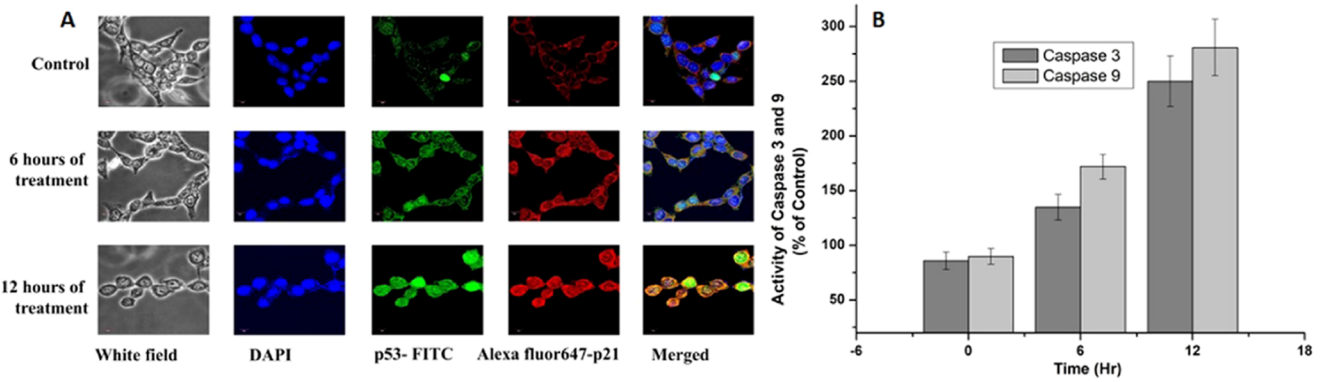

Figure 8. (A) Confocal microscopy images of expression of two main apoptotic markers, p53 and p21. (B) Activity of caspase-3 and caspase-9 with time for **TBOSBL3**-treated HCT-116 cells.

calculated using the Henry law and on the basis of initial slope calculations in the pressure range of 0−0.1 bar (Figures S3 and S4). The CO_2/N_2 selectivity results of **TBOSBL**s are depicted in Table 1. **TBOSBL**s (**TBOSBL1**−**TBOSBL3**) show a reasonably high CO_2/N_2 selectivity (68−108) at 273 K, and this value is better than those of various literature-reported porous materials, such as ACOF-1 (40),[54] TpPa-COF (MW) (32),[55] covalent triazine-based frameworks (CTFs, 20−25),[56] azo-linked polymers (ALPs, 44−60),[57] azine-linked covalent organic frameworks (COF-JLU2, 77),[58] and triptycene-based 1,2,3-triazole-linked networks (31−48).[59] Among the three triptycene-based POPs reported herein, **TBOSBL3** exhibited the highest selectivity (108) for CO_2 over N_2 at 273 K. On the other hand, the CO_2/N_2 selectivity was the lowest for **TBOSBL1** (68) under similar experimental conditions.

A noticeable decrease in CO_2/N_2 selectivity at a higher temperature (298 K) was observed for **TBOSBL2** and **TBOSBL3**, as shown in Table 1. This trend (decreased selectivity at a higher temperature) has commonly been observed for most POPs reported to date.[35] For **TBOSBL1**, the selectivity changes marginally at elevated temperatures (68 at 273 K to 69 at 298 K). The Q_{st} (isosteric heats of adsorption) value of **TBOSBL**s for CO_2 uptake was directly calculated from the experimental adsorption data collected at 273 and 298 K using the Clausius−Clapeyron relation. The Q_{st} values for CO_2 were observed to be in the range 30−35 kJ/mol at zero coverage (Table 1 and Figure 6D). Thus, **TBOSBL**s capture CO_2 via physisorption processes because the magnitude of Q_{st} is less than 40 kJ/mol.[60] The reasonably high Q_{st} value hints at moderate interactions between the polarizable CO_2 molecule (Lewis acidic) and the abundant N−H sites (CO_2-philic and Lewis basic) on the pore wall of **TBOSBL**s via hydrogen bonds. The Q_{st} values of CO_2 for **TBOSBL**s are comparable with those of previous literature-reported porous organic polymers, such as ACOF-1 (27.6 kJ/mol),[54] COF-JLU2 (31 kJ/mol),[58] and TpPa-COF (MW) (34.1 kJ/mol).[55]

2.4. Anticancer Activity of TBOSBLs. A thorough literature survey indicated that there are a handful of reports on porous COFs that demonstrated appreciable anticancer activity against cancer cells, as evident from the low magnitude of IC_{50} values.[22,23,61] Motivated by these results, we too were curious to explore the potential of **TBOSBL**s as antiproliferative agents. To the best of our knowledge, such studies are not known for POPs derived from triptycene-based monomers. Thus, **TBOSBL**s were screened against HCT-116 (human colorectal) cancer cells. Treatment with different concentrations of **TBOSBL**s (0−10 μg/mL) for 6 h amplified the cell death significantly (Figure 7A), and the IC_{50} values were estimated to be 5.01 ± 1.38, 5.71 ± 1.81, and 6.4 ± 1.54 μg/mL for **TBOSBL3**, **TBOSBL2**, and **TBOSBL1** respectively. The IC_{50} values of **TBOSBL**s are lower than that of 5-fluorouracil (a chemotherapeutic drug with IC_{50} = 10.24 ± 2.14 μg/mL). Furthermore, the cytotoxicity of **TBOSBL3** is also superior to those of previous literature-reported porous polymeric materials, such as a triazine-based p-conjugated mesoporous two-dimensional (2D) covalent organic framework—"TrzCOF" (IC_{50} = 8.31 ± 1.67 μg/mL),[61] a porous biodegradable nitrogen containing COF—"EDTFP-1" (IC_{50} = 9.89 ± 1.16 μg/mL),[22] and N-rich porous organic polymer methylenedianiline-triformylphloroglucinol—"MDTFP-1" (IC_{50} = 5.69 ± 1.02 μg/mL).[23] Thus, preliminary experimental investigations revealed that **TBOSBL1**−**3** exhibited appreciable cytotoxicity toward the HCT-116 cell line as per 4,5-(dimethyl-thiazol-2-yl)-2,5-diphenyl tetrazolium bromide (MTT) assay data. The cytotoxicity of **TBOSBL3** is higher than that of **TBOSBL2** and this may be due to a greater pore volume in the former than in the latter. The cytotoxicity of **TBOSBL3** is higher than that of **TBOSBL1** since the former has more functionalized groups. Based on these promising results as obtained from the MTT data, **TBOSBL3** was selected for a further detailed study.

It is well known that an increase in cellular levels of ROS may trigger apoptosis-induced cell death, thereby damaging proteins, nucleic acids, lipids, membranes, and organelles.[62] ROS generation, in turn, may be estimated using 2′,7′-dichlorodihydrofluorescein diacetate (H_2DCFDA), which is a non-fluorescent molecule. In the presence of ROS, H_2DCFDA is oxidized to 2′,7′-dichlorofluorescein (DCF), the latter being a highly fluorescent molecule. It was observed that the mean fluorescence intensity (MFI) of DCF was significantly (P < 0.05) increased in a time-dependent manner upon **TBOSBL3** treatment while checking the extent of ROS generation (Figure 7B). This experiment was repeated several times to confirm the results of ROS generation. To determine whether **TBOSBL3** was involved in apoptosis/necrosis, we have carried out the flow cytometric assessment using annexin V-FITC/propidium iodide (PI) staining by reading the exposed level of phosphatidylserine (PS) in the outer membrane of cells (Figure 7C). It is known that phosphatidylserine (PS) released on the outer leaflet of the plasma membrane is broadly observed during apoptosis.[63] Our result showed that the

https://dx.doi.org/10.1021/acsomega.9b04160
ACS Omega 2020, 5, 4250−4260

percentage of apoptotic (early and late) cells was enhanced in a time-dependent manner (6.2% EA/36.4% LA/39% necrosis for 6 h, 3.4% EA/20.9% LA/50.6% necrosis for 12 h), with respect to the control cells (0.3% EA/0.1% LA/0.0% necrosis) (Figure 7D).

These results hint at **TBOSBL3**-induced cell death that is associated with cytotoxicity followed by apoptosis. We have checked the cytotoxicity of **TBOSBL3** in a normal cell line, namely, human embryonic kidney cells (HEK293), where we detected that the IC_{50} value is 24.7 μg/mL. Thus, from the magnitude of IC_{50}, it may be said that **TBOSBL3** is almost 5 times less active against HEK293 (a normal cell line) relative to HCT-116 (a cancer cell line). Tumor proteins p53 and p21 play a major role in controlling the expression of genes involved in apoptosis.[64] Therefore, after confirmation of ROS-induced apoptosis by **TBOSBL3**, the expression of these two apoptotic markers (p53 and p21) was estimated (Figure 8A). Experimental results suggest that apoptosis was induced in the HCT-116 cells with high levels of p53 expression. The expression of p21 is induced by tumor suppressor gene p53. Our confocal images showed a higher level of p53 and p21 in a time-dependent manner after treatment with **TBOSBL3**, where 4′,6-diamidino-2-phenylindole (DAPI) was used as the fluorescent stain for DNA. Activation of caspase-3 and caspase-9 is required for efficient execution of apoptosis,[65] so we checked the expression of both these caspases. The increased expression of caspase-3 and caspase-9 (Figure 8B) also confirmed that a mitochondria-mediated apoptotic pathway occurred in a time-dependent manner while the cells were treated with **TBOSBL3**.

3. CONCLUSIONS

In summary, this work reports a facile synthesis and characterization of a set of unique triptycene-based and organic Schiff-base-linked polymers (**TBOSBL**s) using 1,3,5-triformylphloroglucinol (TFP). The obtained polymeric networks are characterized using FTIR, NMR, TGA, and XRD. **TBOSBL**s are porous organic polymers (POPs) with a reasonable surface area (SA_{BET} up to 649 m^2/g). **TBOSBL**s have the ability to capture small gas molecules, such as CO_2, H_2, and N_2. While CO_2 uptake capacity is greater than 125 mg/g at 273 K and 1 bar pressure, **TBOSBL**s may be considered as potential materials for molecular hydrogen storage (up to 19.5 mg/g at 77 K and 1 bar pressure). Further, **TBOSBL**s demonstrate very good CO_2/N_2 selectively (up to 108) at 273 K. Inspired by earlier reports of cytotoxicity shown by COFs (bearing phloroglucinol motifs) against cancer cells, **TBOSBL**s are tested to check whether they show any activity against cancer/normal cell lines. Indeed, the measured IC_{50} values for **TBOSBL**s against human colorectal cancer cells are noteworthy. The mechanism of cell death is also studied elaborately. It is explored whether **TBOSBL**s are apoptotic inducers while proposing a mechanism of cell death. **TBOSBL**s are the only example of triptycene-based POPs whose cytotoxic potential against cancer cells have been studied to date. Results of in vitro studies using **TBOSBL**s presented in this work suggest that this new set of POPs have immense potential as anticancer therapeutic agents.

4. EXPERIMENTAL SECTION

4.1. Materials. Triptycene, TFA, and phloroglucinol were purchased from Sigma-Aldrich, and they were used without further purification. Hexamethylene tetramine was procured from CDH. THF was also purchased from Sigma-Aldrich and was dried using common laboratory techniques before use in reactions.

4.2. Instrumentation. Solid-state ^{13}C cross-polarization magic angle spinning (CP-MAS) NMR spectra of **TBOSBL 1−3** were recorded on a Bruker 400 spectrometer equipped with an 89 mm wide bore and a 9.4 T superconducting magnet with a spinning rate of 12 kHz and CP contact time of 2 ms with a delay time of 2 s. FTIR spectra of **TBOSBL 1−3** were collected using a Shimadzu IR Affinity-1 spectrometer. P-XRD analysis data were collected using a Rigaku TTRAX III X-ray diffractometer. TGA plots were recorded using a TG-DSC STA 449 F3 Jupiter (NETZSCH, Selb, Germany) at a scan rate of 10 °C/min under nitrogen flow (100 mL/min). FE-SEM images were obtained using a Carl Zeiss AG instrument (model SUPRA 55). Porosity and surface area were estimated using a Quantachrome Autosorb iQ_2 analyzer. In a typical gas experimental setup, **TBOSBL**s (80−120 mg) were charged in a 9 mm cell and were exposed to degassing at 120 °C for 6−10 h by attaching to a degassing unit. Subsequently, the cells with degassed polymeric samples were filled up with helium gas and weighed accurately for analysis. Various temperatures of the analysis unit sample cell were maintained using a KGW isotherm bath (provided by Quantachrome), which was filled with liquid N_2 (77 K), or a temperature-controlled bath (298 and 273 K).

4.3. Synthesis Procedure of TBOSBLs. *4.3.1. Synthesis of **TBOSBL1**.* Experiments for the synthesis of **TBOSBL**s (Scheme 1) are described using **TBOSBL1** as a typical example. 1,3,5-Triformylphloroglucinol (**1**) (105 mg, 0.5 mmol) and diaminotriptycene (**2**) (214 mg, 0.75 mmol) were dissolved under a flow of nitrogen gas in a solution mixture of dry THF and trifluoroacetic acid (TFA, 2 mol % in THF). The reaction mixture was stirred at 60 °C for 3 days, and the resulting precipitate was collected by suction filtration. The yellow precipitate was washed with tetrahydrofuran, DMF, DMSO, water, methanol, acetone, and dichloromethane, separately. The collected powder was then dried at 120 °C under vacuum for 24 h to yield a yellow powder with 83% isolated yield.

*4.3.2. Synthesis of **TBOSBL2**.* **TBOSBL2** has been synthesized following a similar scheme to that described for **TBOSBL1**. 1,3,5-Triformylphloroglucinol (**1**) (157 mg, 0.75 mmol) and 2,7,14-triaminotriptycene (**3**) (225 mg, 0.75 mmol) were used as monomers for the synthesis of **TBOSBL2**. After drying at reduced pressure at 120 °C, the final product was collected as a yellow powder (yield 81%).

*4.3.3. Synthesis of **TBOSBL3**.* Here, 1,3,5-triformylphloroglucinol (**1**) (157 mg, 0.75 mmol) and 2,6,14-triaminotriptycene (**4**) (225 mg, 0.75 mmol) were used as monomers. The final product was obtained as a yellow powder (yield 80%).

4.4. Cell Culture. Briefly, cells were cultured in Dulbecco's modified Eagle's medium (DMEM) containing 10% fetal bovine serum (FBS) and 1% antibiotic cocktail at 37 °C under constant 5% CO_2 in a humidified condition. After 75−80% confluence, cells were harvested with trypsin (0.25%) and ethylenediaminetetraacetic acid (EDTA, 0.52 mM) in phosphate-buffered saline (PBS) and plated at a necessary density to allow them to re-equilibrate before the experiment.

4.5. Cell Viability. (4,5-Dimethyl-thiazol-2-yl)-2,5-diphenyl tetrazolium bromide (MTT) assay[66] was completed to

https://dx.doi.org/10.1021/acsomega.9b04160
ACS Omega 2020, 5, 4250−4260

estimate cell viability. The cells were plated in 96 well plates and treated with or without different concentrations of **TBOSBL1**, **TBOSBL2**, and **TBOSBL3** for 6 h. Then MTT solution was added. Four hours after the addition of MTT, formazan was solubilized with acidic isopropanol and the absorbance of the solution was measured at 595 nm using an ELISA reader.

4.6. Quantification of Apoptosis Using Flow Cytometry. Apoptotic and necrotic cell death was quantified using the annexin V-FITC/PI apoptosis detection kit (Calbiochem, CA).[67] Briefly, HCT-116 cells were pretreated with 5 μg/mL of **TBOSBL3** for different time durations (6 and 12 h). After an appropriate time period, the cells were washed and stained with PI and annexin V-FITC in accordance with the manufacturer's instructions. The percentages of live, apoptotic (early and late), and necrotic cells were quantified using a flow cytometer (BD LSRFortessa TM San Jose, CA). The acquired data were analyzed.

4.7. Measurement of Intracellular Reactive Oxygen Species (ROS) Generation Using Flow Cytometry. Intracellular ROS accumulation was observed using DCFH-DA, which is a renowned ROS marker. Briefly, **TBOSBL3**-treated cells were incubated with 10 mM DCFH-DA at 37 °C for 25 min, and after that, the cells were analyzed using a flow cytometer (BD LSRFortessa TM San Jose, CA). The acquired data were analyzed.

4.8. Immunofluorescence. Confocal microscopy has been accomplished for observing the expression of two apoptotic markers p53 and p21. Briefly, control/treated HCT-116 cells were washed twice for 10 min each in PBS (0.01 M) and incubated for 1 h in blocking solution having 2% normal bovine serum and 0.3% Triton X-100 in PBS. After blocking, the cells were incubated overnight at 4 °C with the respective primary antibody (p53 and p21), followed by washing and incubation with respective fluorophore-conjugated secondary antibodies (anti mouse/rabbit FITC and Alexa Fluor-647) for 2 h. The slides were then counterstained with 6-diamidino-2-phenylindole (DAPI) for 10 min and mounted with the ProLong antifade reagent (Molecular Probe, Eugene, OR). Stained cells were examined using a confocal laser scanning microscope (FV 10i, Olympus, Japan).

4.9. Caspase-3 and Caspase-9 Activity Assays. The treated cells were subjected to caspase-3 and caspase-9 colorimetric assay using commercially available kits according to the manufacturer's instructions (BioVision Research Products, Mountain View, CA) respectively.

■ ASSOCIATED CONTENT

Supporting Information

The Supporting Information is available free of charge at https://pubs.acs.org/doi/10.1021/acsomega.9b04160.

BET plot of **TBOSBL**s (Figure S1); Langmuir plot of **TBOSBL**s (Figure S2); initial gas uptake slopes of **TBOSBL**s at 273 K (Figure S3); initial gas uptake slopes of **TBOSBL**s at 298 K (Figure S4) (PDF)

■ AUTHOR INFORMATION

Corresponding Author

Neeladri Das − *Department of Chemistry, Indian Institute of Technology Patna, Patna 801106, Bihar, India;* orcid.org/0000-0003-3476-1097; Phone: +91 9631624708; Email: neeladri@iitp.ac.in, neeladri2002@yahoo.co.in

Authors

Akhtar Alam − *Department of Chemistry, Indian Institute of Technology Patna, Patna 801106, Bihar, India*

Snehasis Mishra − *Cancer & Inflammatory Disorder Division, CSIR-Indian Institute of Chemical Biology, Kolkata 700032, India*

Atikur Hassan − *Department of Chemistry, Indian Institute of Technology Patna, Patna 801106, Bihar, India*

Ranajit Bera − *Department of Chemistry, Indian Institute of Technology Patna, Patna 801106, Bihar, India*

Sriparna Dutta − *Department of Chemical Technology, University of Calcutta, Kolkata 700009, West Bengal, India*

Krishna Das Saha − *Cancer & Inflammatory Disorder Division, CSIR-Indian Institute of Chemical Biology, Kolkata 700032, India*

Complete contact information is available at: https://pubs.acs.org/10.1021/acsomega.9b04160

Author Contributions

N.D. conceived the research and supervised the experimental work related to the synthesis and characterization of polymeric materials reported herein. A.A. synthesized all polymeric networks reported in this manuscript. A.H. assisted A.A. in the synthesis of literature-reported monomers. A.A. characterized the polymers and was assisted by R.B. K.D.S. and S.D. supervised the experimental work related to anticancer activities of polymers reported in this manuscript that was performed by S.M. All authors have contributed to the interpretation of respective results, compiled the manuscript, and approved the final manuscript.

Notes

The authors declare no competing financial interest.

■ ACKNOWLEDGMENTS

N.D. thanks the Indian Institute of Technology Patna for providing infrastructure and instrumental facilities required for the research. A.A., A.H., and R.B. thank the Indian Institute of Technology Patna for providing their respective research fellowships. S.M. thanks ICMR for a Senior Research Fellowship. S.M. is also grateful to Tanmoy Dalui, Debalina Chakraborty, Binayak Pal, and Banasri Das of Central Instrumentation Facility, CSIR-Indian Institute of Chemical Biology (IICB), for providing flow cytometer and confocal microscope facilities. S.D. thanks the Department of Chemical Technology, University of Calcutta, for its support. K.D.S. thanks CSIR-IICB for providing research facilities.

■ REFERENCES

(1) Malumbres, M.; Barbacid, M. Cell cycle, CDKs and cancer: a changing paradigm. *Nat. Rev. Cancer* **2009**, *9*, 153−166.

(2) https://www.who.int/news-room/fact-sheets/detail/cancer.

(3) https://www.cancer.net/navigating-cancer-care/cancer-basics/what-cancer.

(4) Naksuriya, O.; Okonogi, S.; Schiffelers, R. M.; Hennink, W. E. Curcumin nanoformulations: A review of pharmaceutical properties and preclinical studies and clinical data related to cancer treatment. *Biomaterials* **2014**, *35*, 3365−3383.

(5) Li, Z.; Yang, Y.-W. Creation and bioapplications of porous organic polymer materials. *J. Mater. Chem. B* **2017**, *5*, 9278−9290.

(6) Wu, J.; Xu, F.; Li, S.; Ma, P.; Zhang, X.; Liu, Q.; Fu, R.; Wu, D. Porous Polymers as Multifunctional Material Platforms toward Task-Specific Applications. *Adv. Mater.* **2019**, *31*, No. 1802922.

(7) Song, Y.; Sun, Q.; Aguila, B.; Ma, S. Opportunities of Covalent Organic Frameworks for Advanced Applications. *Adv. Sci.* **2019**, *6*, No. 1801410.
(8) Zeng, Y.; Zou, R.; Zhao, Y. Covalent Organic Frameworks for CO2 Capture. *Adv. Mater.* **2016**, *28*, 2855−2873.
(9) Zhao, F.; Liu, H.; Mathe, S. D. R.; Dong, A.; Zhang, J. Covalent Organic Frameworks: From Materials Design to Biomedical Application. *Nanomaterials* **2018**, *8*, 15.
(10) Zhang, S.; Yang, Q.; Wang, C.; Luo, X.; Kim, J.; Wang, Z.; Yamauchi, Y. Porous Organic Frameworks: Advanced Materials in Analytical Chemistry. *Adv. Sci.* **2018**, *5*, No. 1801116.
(11) Maity, T.; Saha, D.; Das, S.; Koner, S. Barium Carboxylate Metal−Organic Framework − Synthesis, X-ray Crystal Structure, Photoluminescence and Catalytic Study. *Eur. J. Inorg. Chem.* **2012**, *2012*, 4914−4920.
(12) Rengaraj, A.; Puthiaraj, P.; Haldorai, Y.; Heo, N. S.; Hwang, S.-K.; Han, Y.-K.; Kwon, S.; Ahn, W.-S.; Huh, Y. S. Porous Covalent Triazine Polymer as a Potential Nanocargo for Cancer Therapy and Imaging. *ACS Appl. Mater. Interfaces* **2016**, *8*, 8947−8955.
(13) Wang, Z.; Ma, H.; Zhai, T.-L.; Cheng, G.; Xu, Q.; Liu, J.-M.; Yang, J.; Zhang, Q.-M.; Zhang, Q.-P.; Zheng, Y.-S.; Tan, B.; Zhang, C. Networked Cages for Enhanced CO2 Capture and Sensing. *Adv. Sci.* **2018**, *5*, No. 1800141.
(14) Das, S.; Heasman, P.; Ben, T.; Qiu, S. Porous Organic Materials: Strategic Design and Structure−Function Correlation. *Chem. Rev.* **2017**, *117*, 1515−1563.
(15) Chen, J.-J.; Zhai, T.-L.; Chen, Y.-F.; Geng, S.; Yu, C.; Liu, J.-M.; Wang, L.; Tan, B.; Zhang, C. A triptycene-based two-dimensional porous organic polymeric nanosheet. *Polym. Chem.* **2017**, *8*, 5533−5538.
(16) Ma, H.; Chen, J.-J.; Tan, L.; Bu, J.-H.; Zhu, Y.; Tan, B.; Zhang, C. Nitrogen-Rich Triptycene-Based Porous Polymer for Gas Storage and Iodine Enrichment. *ACS Macro Lett.* **2016**, *5*, 1039−1043.
(17) Zhang, C.; Zhu, P.-C.; Tan, L.; Liu, J.-M.; Tan, B.; Yang, X.-L.; Xu, H.-B. Triptycene-Based Hyper-Cross-Linked Polymer Sponge for Gas Storage and Water Treatment. *Macromolecules* **2015**, *48*, 8509−8514.
(18) Zhang, C.; Liu, Y.; Li, B.; Tan, B.; Chen, C.-F.; Xu, H.-B.; Yang, X.-L. Triptycene-Based Microporous Polymers: Synthesis and Their Gas Storage Properties. *ACS Macro Lett.* **2012**, *1*, 190−193.
(19) Swager, T. M. Iptycenes in the Design of High Performance Polymers. *Acc. Chem. Res.* **2008**, *41*, 1181−1189.
(20) Bera, R.; Ansari, M.; Alam, A.; Das, N. Triptycene, Phenolic-OH, and Azo-Functionalized Porous Organic Polymers: Efficient and Selective CO2 Capture. *ACS Appl. Polym. Mater.* **2019**, *1*, 959−968.
(21) Bera, R.; Ansari, M.; Mondal, S.; Das, N. Selective CO2 capture and versatile dye adsorption using a microporous polymer with triptycene and 1,2,3-triazole motifs. *Eur. Polym. J.* **2018**, *99*, 259−267.
(22) Bhanja, P.; Mishra, S.; Manna, K.; Mallick, A.; Das Saha, K.; Bhaumik, A. Covalent Organic Framework Material Bearing Phloroglucinol Building Units as a Potent Anticancer Agent. *ACS Appl. Mater. Interfaces* **2017**, *9*, 31411−31423.
(23) Bhanja, P.; Mishra, S.; Manna, K.; Das Saha, K.; Bhaumik, A. Porous Polymer Bearing Polyphenolic Organic Building Units as a Chemotherapeutic Agent for Cancer Treatment. *ACS Omega* **2018**, *3*, 529−535.
(24) Zhang, C.; Chen, C.-F. Synthesis and Structure of 2,6,14- and 2,7,14-Trisubstituted Triptycene Derivatives. *J. Org. Chem.* **2006**, *71*, 6626−6629.
(25) Bhadra, M.; Kandambeth, S.; Sahoo, M. K.; Addicoat, M.; Balaraman, E.; Banerjee, R. Triazine Functionalized Porous Covalent Organic Framework for Photo-organocatalytic E−Z Isomerization of Olefins. *J. Am. Chem. Soc.* **2019**, *141*, 6152−6156.
(26) Bhadra, M.; Sasmal, H. S.; Basu, A.; Midya, S. P.; Kandambeth, S.; Pachfule, P.; Balaraman, E.; Banerjee, R. Predesigned Metal-Anchored Building Block for In Situ Generation of Pd Nanoparticles in Porous Covalent Organic Framework: Application in Heterogeneous Tandem Catalysis. *ACS Appl. Mater. Interfaces* **2017**, *9*, 13785−13792.
(27) Shinde, D. B.; Aiyappa, H. B.; Bhadra, M.; Biswal, B. P.; Wadge, P.; Kandambeth, S.; Garai, B.; Kundu, T.; Kurungot, S.; Banerjee, R. A mechanochemically synthesized covalent organic framework as a proton-conducting solid electrolyte. *J. Mater. Chem. A* **2016**, *4*, 2682−2690.
(28) Bera, R.; Ansari, M.; Alam, A.; Das, N. Nanoporous azo polymers (NAPs) for selective CO2 uptake. *J. CO2 Util.* **2018**, *28*, 385−392.
(29) Ansari, M.; Hassan, A.; Alam, A.; Jana, A.; Das, N. Triptycene based fluorescent polymers with azo motif pendants: Effect of alkyl chain on fluorescence, morphology and picric acid sensing. *React. Funct. Polym.* **2020**, *146*, No. 104408.
(30) Ansari, M.; Bera, R.; Mondal, S.; Das, N. Triptycene-Derived Photoresponsive Fluorescent Azo-Polymer as Chemosensor for Picric Acid Detection. *ACS Omega* **2019**, *4*, 9383−9392.
(31) Alam, A.; Bera, R.; Ansari, M.; Hassan, A.; Das, N. Triptycene Based and Amine Linked Nanoporous Networks for Efficient CO2 Capture and Separation. *Front. Energy Res.* **2019**, No. 141.
(32) Deng, G.; Wang, Z. Triptycene-Based Microporous Cyanate Resins for Adsorption/Separations of Benzene/Cyclohexane and Carbon Dioxide Gas. *ACS Appl. Mater. Interfaces* **2017**, *9*, 41618−41627.
(33) Sing, K. S. W. Reporting physisorption data for gas/solid systems with special reference to the determination of surface area and porosity (Provisional). *Pure Appl. Chem.* **1982**, *54*, 2201.
(34) Patel, H. A.; Je, S. H.; Park, J.; Jung, Y.; Coskun, A.; Yavuz, C. T. Directing the Structural Features of N2-Phobic Nanoporous Covalent Organic Polymers for CO2 Capture and Separation. *Chem. - Eur. J.* **2014**, *20*, 772−780.
(35) Arab, P.; Rabbani, M. G.; Sekizkardes, A. K.; İslamoğlu, T.; El-Kaderi, H. M. Copper(I)-Catalyzed Synthesis of Nanoporous Azo-Linked Polymers: Impact of Textural Properties on Gas Storage and Selective Carbon Dioxide Capture. *Chem. Mater.* **2014**, *26*, 1385−1392.
(36) Kandambeth, S.; Mallick, A.; Lukose, B.; Mane, M. V.; Heine, T.; Banerjee, R. Construction of Crystalline 2D Covalent Organic Frameworks with Remarkable Chemical (Acid/Base) Stability via a Combined Reversible and Irreversible Route. *J. Am. Chem. Soc.* **2012**, *134*, 19524−19527.
(37) DeBlase, C. R.; Silberstein, K. E.; Truong, T.-T.; Abruña, H. D.; Dichtel, W. R. β-Ketoenamine-Linked Covalent Organic Frameworks Capable of Pseudocapacitive Energy Storage. *J. Am. Chem. Soc.* **2013**, *135*, 16821−16824.
(38) Kaleeswaran, D.; Vishnoi, P.; Murugavel, R. [3+3] Imine and β-ketoenamine tethered fluorescent covalent-organic frameworks for CO2 uptake and nitroaromatic sensing. *J. Mater. Chem. C* **2015**, *3*, 7159−7171.
(39) Mitra, S.; Kandambeth, S.; Biswal, B. P.; Khayum, M. A.; Choudhury, C. K.; Mehta, M.; Kaur, G.; Banerjee, S.; Prabhune, A.; Verma, S.; Roy, S.; Kharul, U. K.; Banerjee, R. Self-Exfoliated Guanidinium-Based Ionic Covalent Organic Nanosheets (iCONs). *J. Am. Chem. Soc.* **2016**, *138*, 2823−2828.
(40) Bhanja, P.; Das, S. K.; Bhunia, K.; Pradhan, D.; Hayashi, T.; Hijikata, Y.; Irle, S.; Bhaumik, A. A New Porous Polymer for Highly Efficient Capacitive Energy Storage. *ACS Sustainable Chem. Eng.* **2018**, *6*, 202−209.
(41) Li, J.; Cheng, Z.; Zhu, M.; Thomas, A.; Liao, Y. Facile Synthesis of Nitrogen-Rich Porous Organic Polymers for Latent Heat Energy Storage. *ACS Appl. Energy Mater.* **2018**, *1*, 6535−6540.
(42) Dang, Q.-Q.; Wang, X.-M.; Zhan, Y.-F.; Zhang, X.-M. An azo-linked porous triptycene network as an absorbent for CO2 and iodine uptake. *Polym. Chem.* **2016**, *7*, 643−647.
(43) Ghanem, B.; Belmabkhout, Y.; Wang, Y.; Zhao, Y.; Han, Y.; Eddaoudi, M.; Pinnau, I. A unique 3D ultramicroporous triptycene-based polyimide framework for efficient gas sorption applications. *RSC Adv.* **2016**, *6*, 97560−97565.
(44) Zhu, J.-H.; Chen, Q.; Sui, Z.-Y.; Pan, L.; Yu, J.; Han, B.-H. Preparation and adsorption performance of cross-linked porous polycarbazoles. *J. Mater. Chem. A* **2014**, *2*, 16181−16189.

https://dx.doi.org/10.1021/acsomega.9b04160
ACS Omega 2020, 5, 4250−4260

(45) Biswal, B. P.; Chandra, S.; Kandambeth, S.; Lukose, B.; Heine, T.; Banerjee, R. Mechanochemical Synthesis of Chemically Stable Isoreticular Covalent Organic Frameworks. *J. Am. Chem. Soc.* **2013**, *135*, 5328−5331.
(46) Mukherjee, G.; Thote, J.; Aiyappa, H. B.; Kandambeth, S.; Banerjee, S.; Vanka, K.; Banerjee, R. A porous porphyrin organic polymer (PPOP) for visible light triggered hydrogen production. *Chem. Commun.* **2017**, *53*, 4461−4464.
(47) Chandra, S.; Kandambeth, S.; Biswal, B. P.; Lukose, B.; Kunjir, S. M.; Chaudhary, M.; Babarao, R.; Heine, T.; Banerjee, R. Chemically Stable Multilayered Covalent Organic Nanosheets from Covalent Organic Frameworks via Mechanical Delamination. *J. Am. Chem. Soc.* **2013**, *135*, 17853−17861.
(48) Zhu, Y.; Zhang, W. Reversible tuning of pore size and CO2 adsorption in azobenzene functionalized porous organic polymers. *Chem. Sci.* **2014**, *5*, 4957−4961.
(49) Abdelnaby, M. M.; Alloush, A. M.; Qasem, N. A. A.; Al-Maythalony, B. A.; Mansour, R. B.; Cordova, K. E.; Al Hamouz, O. C. S. Carbon dioxide capture in the presence of water by an amine-based crosslinked porous polymer. *J. Mater. Chem. A* **2018**, *6*, 6455−6462.
(50) Fan, C.; Chen, Z.; Pang, L.; Ming, S.; Dong, C.; Brou Albert, K.; Liu, P.; Wang, J.; Zhu, D.; Chen, H.; Li, T. Steam and alkali resistant Cu-SSZ-13 catalyst for the selective catalytic reduction of NOx in diesel exhaust. *Chem. Eng. J.* **2018**, *334*, 344−354.
(51) Yang, Z.; Zhang, H.; Yu, B.; Zhao, Y.; Ma, Z.; Ji, G.; Han, B.; Liu, Z. Azo-functionalized microporous organic polymers: synthesis and applications in CO2 capture and conversion. *Chem. Commun.* **2015**, *51*, 11576−11579.
(52) Lee, S.-P.; Mellon, N.; Shariff, A. M.; Leveque, J.-M. Geometry variation in porous covalent triazine polymer (CTP) for CO2 adsorption. *New J. Chem.* **2018**, *42*, 15488−15496.
(53) Liao, Y.; Weber, J.; Mills, B. M.; Ren, Z.; Faul, C. F. J. Highly Efficient and Reversible Iodine Capture in Hexaphenylbenzene-Based Conjugated Microporous Polymers. *Macromolecules* **2016**, *49*, 6322−6333.
(54) Li, Z.; Feng, X.; Zou, Y.; Zhang, Y.; Xia, H.; Liu, X.; Mu, Y. A 2D azine-linked covalent organic framework for gas storage applications. *Chem. Commun.* **2014**, *50*, 13825−13828.
(55) Wei, H.; Chai, S.; Hu, N.; Yang, Z.; Wei, L.; Wang, L. The microwave-assisted solvothermal synthesis of a crystalline two-dimensional covalent organic framework with high CO2 capacity. *Chem. Commun.* **2015**, *51*, 12178−12181.
(56) Dey, S.; Bhunia, A.; Esquivel, D.; Janiak, C. Covalent triazine-based frameworks (CTFs) from triptycene and fluorene motifs for CO2 adsorption. *J. Mater. Chem. A* **2016**, *4*, 6259−6263.
(57) Arab, P.; Parrish, E.; İslamoğlu, T.; El-Kaderi, H. M. Synthesis and evaluation of porous azo-linked polymers for carbon dioxide capture and separation. *J. Mater. Chem. A* **2015**, *3*, 20586−20594.
(58) Li, Z.; Zhi, Y.; Feng, X.; Ding, X.; Zou, Y.; Liu, X.; Mu, Y. An Azine-Linked Covalent Organic Framework: Synthesis, Characterization and Efficient Gas Storage. *Chem. - Eur. J.* **2015**, *21*, 12079−12084.
(59) Mondal, S.; Das, N. Triptycene based 1,2,3-triazole linked network polymers (TNPs): small gas storage and selective CO2 capture. *J. Mater. Chem. A* **2015**, *3*, 23577−23586.
(60) Patel, H. A.; Hyun Je, S.; Park, J.; Chen, D. P.; Jung, Y.; Yavuz, C. T.; Coskun, A. Unprecedented high-temperature CO2 selectivity in N2-phobic nanoporous covalent organic polymers. *Nat. Commun.* **2013**, *4*, No. 1357.
(61) Kanti Das, S.; Mishra, S.; Manna, K.; Kayal, U.; Mahapatra, S.; Das Saha, K.; Dalapati, S.; Das, G. P.; Mostafa, A. A.; Bhaumik, A. A new triazine based π-conjugated mesoporous 2D covalent organic framework: its in vitro anticancer activities. *Chem. Commun.* **2018**, *54*, 11475−11478.
(62) Redza-Dutordoir, M.; Averill-Bates, D. A. Activation of apoptosis signalling pathways by reactive oxygen species. *Biochim. Biophys. Acta, Mol. Cell Res.* **2016**, *1863*, 2977−2992.
(63) Lee, S. H.; Meng, X. W.; Flatten, K. S.; Loegering, D. A.; Kaufmann, S. H. Phosphatidylserine exposure during apoptosis reflects bidirectional trafficking between plasma membrane and cytoplasm. *Cell Death Differ.* **2013**, *20*, 64−76.
(64) Li, T.; Kon, N.; Jiang, L.; Tan, M.; Ludwig, T.; Zhao, Y.; Baer, R.; Gu, W. Tumor Suppression in the Absence of p53-Mediated Cell-Cycle Arrest, Apoptosis, and Senescence. *Cell* **2012**, *149*, 1269−1283.
(65) Brentnall, M.; Rodriguez-Menocal, L.; De Guevara, R. L.; Cepero, E.; Boise, L. H. Caspase-9, caspase-3 and caspase-7 have distinct roles during intrinsic apoptosis. *BMC Cell Biol.* **2013**, *14*, 32.
(66) Mosmann, T. Rapid colorimetric assay for cellular growth and survival: Application to proliferation and cytotoxicity assays. *J. Immunol. Methods* **1983**, *65*, 55−63.
(67) Dey, S. K.; Bose, D.; Hazra, A.; Naskar, S.; Nandy, A.; Munda, R. N.; Das, S.; Chatterjee, N.; Mondal, N. B.; Banerjee, S.; Saha, K. D. Cytotoxic Activity and Apoptosis-Inducing Potential of Di-spiropyrrolidino and Di-spiropyrrolizidino Oxindole Andrographolide Derivatives. *PLoS One* **2013**, *8*, No. e58055.

https://dx.doi.org/10.1021/acsomega.9b04160
ACS Omega 2020, 5, 4250−4260